Throughput analysis of RIS-assisted UAV wireless systems under disorientation and misalignment

Alexandros-Apostolos Boulogeorgos, Angeliki Alexiou, Marco Di Renzo

HAL Id: hal-04262664
https://hal.science/hal-04262664

Submitted on 27 Oct 2023

Throughput analysis of RIS-assisted UAV wireless systems under disorientation and misalignment

Alexandros-Apostolos A. Boulogeorgos [1], Angeliki Alexiou [1], and Marco Di Renzo [2]

[1]Digital Systems, University of Piraeus Piraeus 18534 Greece. e-mails: al.boulogeorgos@ieee.org, alexiou@unipi.gr.
[2]Université Paris-Saclay, CNRS, CentraleSupélec, Laboratoire des Signaux et Systèmes, 3 Rue Joliot-Curie, 91192 Gif-sur-Yvette, France.
e-mail: marco.di-renzo@universite-paris-saclay.fr

Abstract—Reconfigurable intelligent surface (RIS)-assisted unmanned areal vehicles (UAV) communications have been identified as a key enabler of a number of next-generation applications. However, to the best of our knowledge, there is no generalized framework for the quantification of the throughput performance of RIS-assisted UAV systems. Motivated by this, in this paper, we present a comprehensive system model that accounts the impact of multi-path fading, which is modeled by means of mixture gamma, transceiver hardware imperfections, and stochastic beam disorientation and misalignment in order to examine the throughput performance of a RIS-assisted UAV wireless system. In this direction, we present a novel closed-form expression for the systems throughput for two scenarios: i) in the presence and ii) in the absence of disorientation and misalignment. Interestingly, our results reveal the importance of accurate modeling the aforementioned phenomena as well as the existence of an optimal transmission spectral efficiency.

Index Terms—Hardware imperfections, performance analysis, reconfigurable intelligent surfaces, statistical characterization, unmanned areal vehicles.

I. INTRODUCTION

Unmanned aerial vehicles (UAVs) have been widely recognized as one of the key enablers of beyond the fifth generation (B5G) networks [2], [3]. From communications point of view, all UAV-based system models have two common requirements: i) ultra-reliable connectivity [4], [5], and ii) high-energy efficiency [6]–[8]. These requirements can be technically translated into the necessity of creating a beneficial and reconfigurable electromagnetic environment without decreasing the UAV's energy efficiency.

Recognizing the aforementioned need, several researchers have recently focused their attention on combining UAVs and reconfigurable intelligent surfaces (RIS) [9]–[12]. In more detail, in [9], the performance of an interference-limited RIS-assisted UAV wireless system suffering from Nakagami-m fading was evaluated in terms of coverage probability, bit and block error rates. In [10], the active beamforming of the UAV, the coefficients of the RIS MAs, and the trajectory of the UAV were jointly optimized to maximize the overall secrecy rate of all legitimate users in the presence of multiple

eavesdroppers in RIS-assisted UAV wireless systems operating in the millimeter-wave band and exhibiting Rayleigh fading. In [11], the authors investigated the joint optimization of UAV trajectory, RIS PS, sub-band allocation, and power management to maximize the minimum average achievable rate of all users in a RIS-assisted UAV wireless system operating in the terahertz (THz) band. Finally, in [12], the OP, average bit error rate, and ergodic capacity of RIS-assisted dual-hop UAV communication systems were quantified, where the S-RIS and RIS-UAV links were modeled as Rayleigh and mixture-Gamma (MG) RVs, respectively.

To the best of the authors' knowledge, no generalized channel model has yet been presented that captures the specifics of RIS-assisted UAV wireless systems and enables performance evaluation in different propagation environments. Likewise, most of the aforementioned contributions assume that the RIS-UAV link is not directional. As a result, the detrimental effect of UAV disorientation and/or misalignment of the RIS-UAV beam have been neglected. However, as we move toward higher operating frequency, the directionality of links is expected to increase [5], [13]–[15]. Hence, even small disorientations and/or misalignments may adversely affect the performance of the RIS-assisted UAV wireless system. Aside from the joint effect of disorientation and misalignment, another important performance-limiting factor in high-frequency communications is the effect of transceiver hardware imperfections [16]–[18].

Motivated by this, this work derives a generalized framework for evaluating the throughput performance of RIS-assisted UAV wireless systems that captures the effects of various fading conditions, disorientation, misalignment, and/or hardware imperfections. The technical contribution lies in the presentation of a comprehensive system model that accounts for the effects of various small-scale fading conditions, the joint effect of stochastic disorientation and misalignment, as well as transceiver hardware imperfections. In contrast to previous publications, we assume independent MG fading in both S-RIS and RIS-UAV channels. Moreover, we closed-form expressions, simplified for the following cases: (i) the RIS-UAV link experience neither disorientation nor misalignment, (ii) the RIS-UAV link experience disorientation and misalignment.

Notations: Unless otherwise stated, lower bold letter stands for vectors. $\Pr(\mathcal{A})$ denotes the probability for the event

Fig. 1: System model

Fig. 2: The relative position and orientation of the RIS and UAV in the considered coordinate systems.
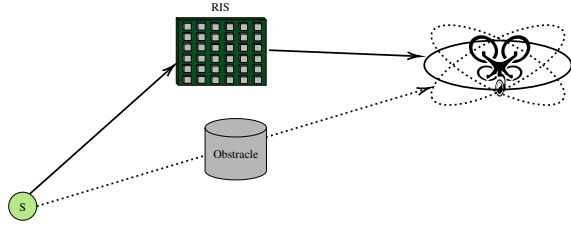
$\mathcal{A}$ to be valid. Likewise, $\cos(x)$ gives the cosine of x, while $\sin(x)$ returns the sine of x. Moreover, $\csc(x)$ stands for the cosecant of x. The error-function is represented by $\mathrm{erf}(\cdot)$ [19, eq. (8.250/1)]. The modified Bessel function of the second kind of order n is denoted as $\mathrm{K}_n(\cdot)$ [19, Eq. (8.407/1)]. The Gamma [19, Eq. (8.310)] function is denoted by $\Gamma(\cdot)$. Finally, $_pF_q(a_1, a_2, \cdots, a_p; b_1, b_2, \cdots, b_q; x)$ and $G_{p,q}^{m,n}\left(x \left| \begin{array}{c} a_1, a_2, \cdots, a_p \\ b_1, b_2, \cdots, b_q \end{array} \right. \right)$ respectively stand for the generalized hypergeometric function [19, Eq. (9.111)] and the Meijer G-function [19, Eq. (9.301)].

II. SYSTEM MODEL

As shown in Fig. 1, we consider an RIS-assisted UAV wireless system in which the S communicates with a UAV via a RIS. We assume that no direct link can be established between S and the UAV, due to the presence of blockage. It is assumed that the UAV is in a hover state, where, in practice, both the position and orientation of the UAV are not completely fixed. It is also assumed that both the S and the UAV are equipped with single antennas, while the RIS consists of N MAs. To determine the relative position and orientation of the RIS and the UAV, we define two three-dimensional Cartesian coordinate systems, as demonstrated in Fig. 2. The RIS is assumed to be at the origin of the Cartesian coordinate system (x, y, z), i.e., at position $(0, 0, 0)$. At a specific timeslot, it is assumed that the UAV is located at position $\mathbf{d}_\epsilon = (d_x + \epsilon_x, d_y + \epsilon_y, d_z + \epsilon_z)$, with respect to the (x, y, z) coordinate system, where $\mathbf{d} = (d_x, d_y, d_z)$ denotes the mean of the random vector $\mathbf{d}_\epsilon$ and $\boldsymbol{\epsilon} = (\epsilon_x, \epsilon_y, \epsilon_z)$ are independent and identical zero-mean Gaussian distributed RVs with variance σ_p^2. For a given $\mathbf{d}_\epsilon$, a second Cartesian coordinate system (x', y', z'), for which $\mathbf{d}_\epsilon$ is at the origin and the axes x', y', and z' are parallel with the axes x, y, and z, respectively, is considered. Let $\theta_\epsilon \in [0, 2\pi]$ be the angle between the axis x' and the projection of the beam vector onto the $x' - y'$ plane. Similarly, $\phi_\epsilon \in [0, \pi]$ represents the angle between the z' axis and the beam vector. Notice that both θ_ϵ and ϕ_ϵ are randomly distributed variables that can be respectively expressed as $\theta_\epsilon = \theta + \epsilon_\theta$ and $\phi_\epsilon = \phi + \epsilon_\phi$, where θ and ϕ denote the mean of θ_ϵ and ϕ_ϵ, respectively, while ϵ_θ and ϵ_ϕ are zero-mean RVs with variance σ_o^2.

By h_i and g_i we denote the complex coefficients of the S to $i-$th MA and $i-$th MA to UAV baseband equivalent fading channels, respectively. It is assumed that all the fading channels considered are independent, identical, slowly varying, and flat. Finally, we use θ_i to denote the response of the $i-$th
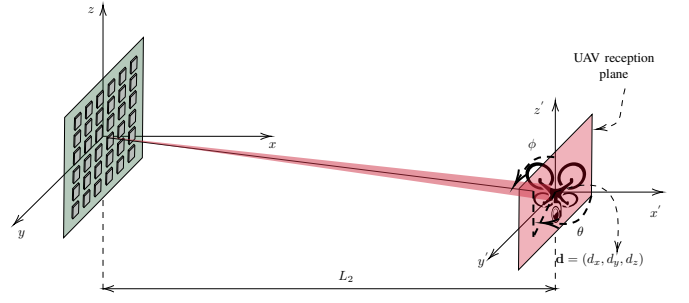
MA. As a result, the baseband equivalent received signal at D can be obtained as

$$r = \begin{cases} h_l\, A\,(s + \eta_s) + \eta_d + w, & \text{without disorientation} \\ & \text{or misalignment} \\ h_l\, h_g\, A\,(s + \eta_s) + \eta_d + w, & \text{with disorientation} \\ & \text{and misalignment} \end{cases} \quad (1)$$

where s represents the S transmission symbol, while w stands for the additive white Gaussian noise (AWGN), which is modeled as a zero-mean complex Gaussian (ZMCG) RV with variance equal to σ_w^2. Moreover, h_l denotes the e2e spreading-loss coefficient and can be written as $h_l = h_{l,1}\, h_{l,2}$, where

$$h_{l,i} = l_i\, L_i^{-n_i/2}, \text{ with } i \in \{1, 2\}, \quad (2)$$

is the spreading loss coefficient of the S-RIS ($i = 1$) and RIS-UAV ($i = 2$) links respectively. In (2), l_1 and l_2 respectively denote the square root of the reference reception power, while n_1 and n_2 stand for the path-loss exponent of the S-RIS and RIS-UAV links, respectively. The transmission distances of the S-RIS and RIS-D links are denoted by L_1 and L_2, respectively.

In addition, h_g represents the geometric-loss caused by the disorientation of the UAV and the misalignment of the beam between the RIS and the UAV. According to [20], the PDF of h_g can be expressed as

$$f_{h_g}(x) = \frac{\rho}{B_o}\left(\frac{x}{B_o}\right)^{\zeta-1}, \text{ with } 0 \le x \le B_o. \quad (3)$$

In (3), $B_o = \mathrm{erf}(v_{\min})\,\mathrm{erf}(v_{\max})$, where

$$v_i = \frac{\alpha}{w(L_2)}\sqrt{\frac{\pi}{2\rho_i}}, \text{ with } i \in \{\min, \max\}. \quad (4)$$

In (4), $\rho_{\min} = \frac{2}{\rho_y + \rho_z + \sqrt{(\rho_y - \rho_z)^2 + 4\rho_{zy}^2}}$ and $\rho_{\max} = \frac{2}{\rho_y + \rho_z - \sqrt{(\rho_y - \rho_z)^2 + 4\rho_{zy}^2}}$ where $\rho_y = \cos^2(\phi) + \sin^2(\phi)\cos^2(\theta)$, $\rho_z = \sin^2(\phi)$ and $\rho_{yz} = -\cos(\phi)\sin(\phi)\sin(\theta)$. Moreover, α is the radius of the UAV antenna effective area, while $w(L_2)$ is the RIS beamwidth at distance L_2 and can be expressed as $w(L_2) = w_o\sqrt{1 + \left(1 + \frac{2w_o^2}{\rho^2(L_2)}\right)\left(\frac{cL_2}{\pi f w_o^2}\right)^2}$, with w_o being the beam-waist radius, c denoting the speed of light, f standing for the transmission frequency, and $\rho(L_2)$ representing the coherence length. Of note, the coherence length can be evaluated as $\rho(L_2) = \left(0.55\, C_n^2\, k^2\, L_2\right)^{-3/5}$,

where C_n^2 stands for the index of refraction structure parameter and $k = \frac{2\pi f}{c}$, is the wave-number. In (3), $\zeta = \frac{k_m (w(L_2))^2}{4\sigma_p^2 + 4d_x^2 \sigma_0^2}$. with $k_m = \frac{k_{\min} + k_{\max}}{2}$, where $k_i = \frac{\sqrt{\pi}\rho_i \operatorname{erf}(v_i)}{2v_i \exp(-v_i^2)}$, with $i \in \{\min, \max\}$.

Finally,

$$A = \sum_{i=1}^{N} h_i \theta_i g_i, \tag{5}$$

where h_i and g_i are the S-i−th MA and i−th MA-D channel coefficients, which can be expressed as

$$h_i = |h_i| \exp(j\phi_{h_i}) \text{ and } g_i = |g_i| \exp(j\phi_{g_i}), \tag{6}$$

with ϕ_{h_i} and ϕ_{g_i} respectively being the phases of h_i and g_i. The envelops of h_i and g_i are assumed to be independent MG random variables with PDFs that can be respectively expressed as

$$f_{h_i}(x) = \sum_{m=1}^{M} 2a_m^{(1)} x^{2b_m^{(1)}-1} \exp\left(-c_1 x^2\right) \tag{7}$$

and

$$f_{g_i}(x) = \sum_{k=1}^{K} 2a_k^{(2)} x^{2b_k^{(2)}-1} \exp\left(-c_2 x^2\right), \tag{8}$$

where M and K are the numbers of terms for the approximation of the PDF of $|h_i|$ and $|g_i|$, respectively, while $a_m^{(1)}$, $b_m^{(1)}$ and c_1 with $m \in [1, M]$ are parameters of the m−th term of (7). Similarly, $a_k^{(2)}$, $b_k^{(2)}$ and c_2 with $k \in [1, K]$ are parameters of the k−th term of (8).

Moreover, in (5), θ_i stands for the i−th MA response and can be further written as

$$\theta_i = |\theta_i| \exp\left(j\phi_i\right), \tag{9}$$

with $|\theta_i|$ and ϕ_i respectively representing the i−th MA response gain and the PS applied by the i−th MA of the RIS. Without loss of generality, we assume that $|\theta_i| = 1$. Based on [21], this is considered a realistic assumption. As reported in several works including [22], [23], the optimal PS for the i−th MA is

$$\phi_i = -\phi_{h_i} - \phi_{g_i}. \tag{10}$$

By applying (10) to (5), we get

$$A = \sum_{i=1}^{N} |h_i| |g_i|. \tag{11}$$

In (1), η_s and η_d models respectively for the impact of S and UAV RF chains hardware imperfections. According to [24], [25], for a given e2e channel realization, η_s and η_d can be modeled as two independent ZMCG RVs with variances that can be respectively expressed as $\sigma_s^2 = \kappa_t^2 P_s$ and $\sigma_d^2 = \kappa_r^2 h_l^2 h_g^2 A^2 P_s$, where κ_t and κ_r are respectively the S transmitter and UAV receiver error vector magnitudes, while P_s stands for the average transmitted power. According to [26], [27], κ_t and κ_r in high-frequency systems, such as millimeter wave and terahertz (THz), are in the range of $[0.07, 0.3]$. Finally, for the special case in which both the S and UAV are equipped with ideal transceivers, $\kappa_t = \kappa_r = 0$ [28].

III. THROUGHPUT ANALYSIS

The signal-to-distortion-plus-noise-ratio (SDNR) at the UAV can be expressed as

$$\gamma_u = \begin{cases} \frac{h_l^2 A^2 P_s}{(\kappa_t^2 + \kappa_r^2) h_l^2 A^2 P_s + \sigma_w^2}, & \text{without disorientation} \\ & \text{or misalignment} \\ \frac{h_l^2 A_{e2e}^2 P_s}{(\kappa_t^2 + \kappa_r^2) h_l^2 A_{e2e}^2 P_s + \sigma_w^2}, & \text{with disorientation} \\ & \text{and misalignment} \end{cases} \tag{12}$$

or equivalently

$$\gamma_u = \begin{cases} \frac{A^2}{(\kappa_t^2 + \kappa_r^2) A^2 + \frac{1}{\gamma}}, & \text{without disorientation} \\ & \text{or misalignment} \\ \frac{A_{e2e}^2}{(\kappa_t^2 + \kappa_r^2) A_{e2e}^2 + \frac{1}{\gamma}}, & \text{with disorientation} \\ & \text{and misalignment} \end{cases} \tag{13}$$

A. Without disorientation and misalignment

The following proposition returns the throughput in the absence of disorientation and misalignment.

Proposition 1. *In the absence of both disorientation and misalignment, the throughput can be evaluated as*

$$\mathcal{D}^{wo}(r_{\text{th}}) = \begin{cases} r_{\text{th}}\left(1 - \dfrac{\mathrm{G}_{1,3}^{2,1}\left(\left.\dfrac{\Xi^2 \frac{2^{r_{\text{th}}}-2}{\gamma}}{1-(\kappa_t^2+\kappa_r^2)(2^{r_{\text{th}}}-1)}\right| \begin{matrix} 1 \\ k_A, m_A, 0 \end{matrix}\right)}{\Gamma(k_A)\Gamma(m_A)}\right), \\ \qquad\qquad \text{for } r_{\text{th}} < \log_2\left(\frac{1}{\kappa_t^2+\kappa_r^2}+1\right) \\ 0, \qquad\quad \text{for } r_{\text{th}} \geq \log_2\left(\frac{1}{\kappa_t^2+\kappa_r^2}+1\right) \end{cases} \tag{14}$$

where

$$k_A = -\frac{b_A}{2a_A} + \frac{\sqrt{b_A^2 - 4a_A c_A}}{2a_A}, \tag{15}$$

$$m_A = -\frac{b_A}{2a_A} - \frac{\sqrt{b_A^2 - 4a_A c_A}}{2a_A} \tag{16}$$

and

$$\Xi = \sqrt{\frac{k_A m_A}{\Omega_A}}. \tag{17}$$

In (15)–(17),

$$a_A = \mu_A(6)\mu_A(2) + (\mu_A(2))^2 \mu_A(4) - 2(\mu_A(4))^2, \tag{18}$$

$$b_A = \mu_A(6)\mu_A(2) - 4(\mu_A(4))^2 + 3(\mu_A(2))^2 \mu_A(4), \tag{19}$$

$$c_A = 2(\mu_A(2))^2 \mu_A(4) \tag{20}$$

and

$$\Omega_A = \mu_A(2), \tag{21}$$

where

$$\mu_A(l) = \sum_{l_1=0}^{l} \sum_{l_2=0}^{l_1} \cdots \sum_{l_{N-1}=0}^{l_{N-2}} \binom{l}{l_1} \binom{l_1}{l_2} \cdots \binom{l_{N-2}}{l_{N-1}} \\ \times \mu_{\chi_1}(l - l_1) \mu_{\chi_2}(l_1 - l_2) \cdots \mu_{\chi_{N-1}}(l_{N-1}) \tag{22}$$

and

$$\mu_{\chi_i}(l) = \sum_{m=1}^{M} \sum_{k=1}^{K} a_m^{(1)} a_k^{(2)} \left(\frac{c_1}{c_2}\right)^{-\frac{b_m^{(1)} - b_k^{(2)}}{2}} (c_1 c_2)^{-\frac{b_m^{(1)} + b_k^{(2)} + n}{2}} \\ \times \Gamma\left(b_m^{(1)} + \frac{n}{2}\right) \Gamma\left(b_k^{(2)} + \frac{n}{2}\right) \tag{23}$$

Proof: For brevity, the proof of Proposition 1 is provided in Appendix A. ∎

Remark 1. From (14), it becomes apparent that a maximum transmission spectral efficiency threshold exists that is equal to

$$r_{\text{th}}^m = 2^{\frac{1}{\kappa_t^2 + \kappa_r^2}} - 1, \tag{24}$$

beyond which the throughput becomes equal to 0. Interestingly, r_{th}^m only depends on the levels of hardware imperfections of the S's transmitter and UAV's receiver.

B. With disorientation and misalignment

The following proposition returns the thoughput in the presence of disorientation and misalignment.

Proposition 2. *In the presence of disorientation and misalignment, the throughput can be assessed as in* (25), *given at the top of the next page.*

Proof: For brevity, the proof of proposition 2 is given in Appendix B. ∎

IV. RESULTS & DISCUSSION

This section is devoted to verify the theoretical framework that has been presented in Section III, by means of Monte Carlo simulations and provide an insightful discussion of the effects of fading, disorientation and misalignment in RIS-assisted UAV wireless systems. Along these lines, the following insightful scenario is considered. It is assumed that S-RIS channel coefficients follow independent and identical Nakagami-m distributions with spread parameters $\Omega = 1$; thus, $M = 1$, $a_1^{(1)} = \frac{m^m}{\Gamma(m)}$, $b_1^{(1)} = m$, and $c_1 = m$, where m represents the shape parameter. The Rice distribution is used to model the channel coefficients of the RIS-UAV link. For an accurate approximation of the Rice distribution, we select $K = 20$,

$$a_k^{(2)} = \frac{\delta(K_r, k)}{\sum_{k_1=1}^{K} \delta(K_r, k_1) \Gamma\left(b_{k_1}^{(2)}\right) c_2^{-b_{k_1}^{(2)}}}, \tag{26}$$

where

$$\delta(K_r, k) = \frac{K_r^{k-1}(1 + K_r)^k}{\exp(K_1)((n-1)!)^2}, \tag{27}$$

while $c_2 = 1 + K_r$, and $b_k^{(2)} = k$. Moreover, note that in (26), K_r stands for the $K-$factor of the Rice distribution. Unless otherwise stated, the following scenario is considered. The transmission frequency is set to 100 GHz, $L_1 = 10$ m and $L_2 = 5$ m. Moreover, $w_o = 1$ mm, $\theta = -\frac{\pi}{4}$ and $\phi = \frac{4\pi}{3}$, while $\sigma_p = 0.05$ rad, $\sigma_o = 0.1$ rad, and $d_x = 0.1$. Finally, $N = 16$ and $K = 5$ dB.

Figure 3 quantifies the impact of transceivers hardware imperfections on the throughput performance of the RIS-assisted UAV wireless system. In particular, the achievable throughput is plotted as a function of r_{th}, for different values of γ and $\kappa_t = \kappa_r$. From this figure, it becomes evident that for given $\kappa_t = \kappa_r$ and γ, an optimal transmission scheme

spectral efficiency exists, r_{th}^*. For $r_{\text{th}} < r_{\text{th}}^*$, the achievable throughput increases, as r_{th} increases. On the other hand, for $r_{\text{th}} > r_{\text{th}}^*$, the achievable throughput decreases, as r_{th} increases. Moreover, for fixed r_{th} and $\kappa_t = \kappa_r$, as γ increases, the achievable throughput also increases. For example, for $r_{\text{th}} = 3$ bits/s/Hz and $\kappa_t = \kappa_r = 0.1$, the achievable throughput increases from 2.72 to 3 bits/s/Hz, as γ increases from -5 to 5 dB. Finally, for given γ and r_{th}, as the level of transceiver hardware imperfections increases, an achievable throughput degradation is observed.

Figure 4 depicts the achievable throughput as a function of L_2, for different values of γ and $\kappa_t = \kappa_r$, assuming $r_{\text{th}} = 2$ bits/s/Hz. As expected, for given $\kappa_t = \kappa_r$ and γ, as L_2 increases, the impact of disorientation becomes more severe; thus, the throughput decreases. For example, for $\kappa_t = \kappa_r = 0$, i.e., the ideal RF front-end case, and $\gamma = -5$ dB, the throughput decreases from 1.9 to 0 bits/s/Hz, as L_2 increases from 10 to 100 m. Moreover, for fixed L_2 and γ, as the level of transceiver hardware imperfections increases, the achievable throughput decreases. For instance, for $L_2 = 50$ m and $\gamma = -5$ dB, the achievable throughput changes from 0.49 to 0.42 bits/s/Hz, as $\kappa_t = \kappa_r$ increases from 0 to 0.1. Finally, for given L_2 and $\kappa_t = \kappa_r$, the achievable throughput increases, as γ increases.

V. CONCLUSIONS

This paper was devoted to analyze the throughput performance of RIS-assisted UAV wireless systems in the absence and presence of stochastic beam misalignment and disorientation as well as transceiver hardware imperfections. In this direction, novel closed-form expressions for the achievable throughput for both cases of presence and absence of stochastic beam misalignment and disorientation were derived. Our results highlighted the importance of accurate modeling the aforementioned phenomena as well as small-scale fading, when assessing the throughput performance of RIS-assisted UAV wireless systems. Finally, it became evident that an optimal transmission spectral efficiency exists for which the achievable throughput is maximized.

APPENDICES

APPENDIX A

PROOF OF PROPOSITION 1

The throughput is defined as

$$\mathcal{D}^{\text{wo}}(r_{\text{th}}) = r_{\text{th}} \Pr(r > r_{\text{th}}), \tag{28}$$

where

$$r = \log_2(1 + \gamma_u). \tag{29}$$

In the absence of disorientation and misalignment, (29) can be rewritten as

$$r = \log_2\left(1 + \frac{A^2}{(\kappa_t^2 + \kappa_r^2) A^2 + \frac{1}{\gamma}}\right). \tag{30}$$

$$\mathcal{D}^{\text{w}}(r_{\text{th}}) = \begin{cases} r_{\text{th}}\left(1 - \dfrac{\zeta G_{5,3}^{1,4}\left(\begin{matrix} 1-k_A, 1-m_A, \frac{1-\zeta}{2}, \frac{2-\zeta}{2}, 1 \\ 0, \frac{1-\zeta}{2}, -\frac{\zeta}{2} \end{matrix} \,\middle|\, \frac{B^2}{\Xi^2}\frac{\gamma}{2^{r_{\text{th}}}-1}\right)}{2\Gamma(k_A)\Gamma(m_A)}\right), & \text{for } r_{\text{th}} < \log_2\left(\frac{1}{\kappa_t^2+\kappa_r^2}+1\right) \\[4mm] 0, & \text{for } r_{\text{th}} \geq \log_2\left(\frac{1}{\kappa_t^2+\kappa_r^2}+1\right) \end{cases} \qquad (25)$$
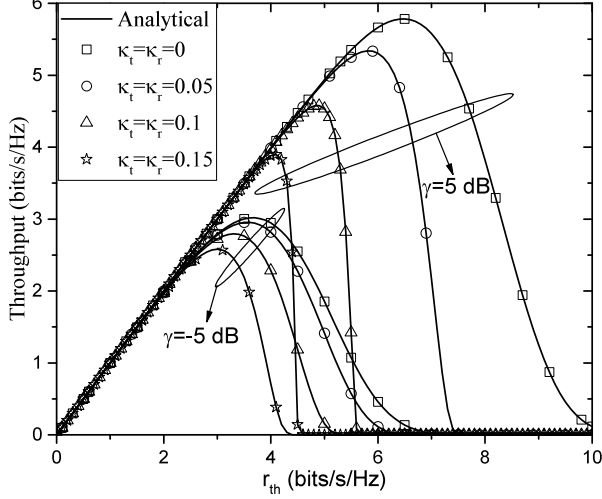

Fig. 3: Throughput vs r_{th}, for different values of γ and $\kappa_t = \kappa_r$.

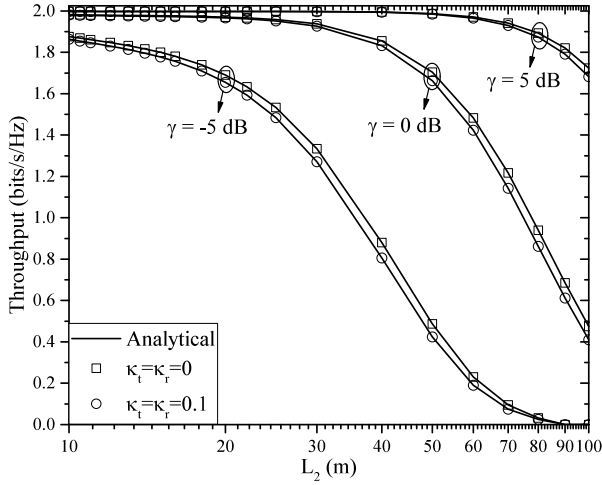
Fig. 4: Throughput vs L_2, for different values of γ and $\kappa_t = \kappa_r$.

By applying (30) into (28), the throughput can be rewritten as

$$\mathcal{D}^{\text{wo}}(r_{\text{th}}) = r_{\text{th}}\Pr\left(\log_2\left(1 + \frac{A^2}{(\kappa_t^2+\kappa_r^2)A^2+\frac{1}{\tilde{\gamma}}}\right) > r_{\text{th}}\right), \qquad (31)$$

or equivalently

$$\mathcal{D}^{\text{wo}}(r_{\text{th}}) = r_{\text{th}}$$
$$\times \Pr\left(A^2\left(1 - (2^{r_{\text{th}}}-1)\left(\kappa_t^2+\kappa_r^2\right)\right) > \frac{2^{r_{\text{th}}}-1}{\tilde{\gamma}}\right) \qquad (32)$$

or

$$\mathcal{D}^{\text{wo}}(r_{\text{th}}) = r_{\text{th}}$$
$$\times \left(1 - \Pr\left(A^2\left(1 - (2^{r_{\text{th}}}-1)\left(\kappa_t^2+\kappa_r^2\right)\right) \leq \frac{2^{r_{\text{th}}}-1}{\tilde{\gamma}}\right)\right). \qquad (33)$$

For $(2^{r_{\text{th}}}-1)\left(\kappa_t^2+\kappa_r^2\right) > 1$, $A^2\left(1 - (2^{r_{\text{th}}}-1)\left(\kappa_t^2+\kappa_r^2\right)\right)$ is always negative, thus, $\Pr\left(A^2\left(1 - (2^{r_{\text{th}}}-1)\left(\kappa_t^2+\kappa_r^2\right)\right) \leq \frac{2^{r_{\text{th}}}-1}{\tilde{\gamma}}\right) = 1$, and

$$\mathcal{D}^{\text{wo}}(r_{\text{th}}) = 0, \text{ for } r_{\text{th}} > \log_2\left(1 + \frac{1}{\kappa_t^2+\kappa_r^2}\right). \qquad (34)$$

On the other hand, for $r_{\text{th}} < \log_2\left(1 + \frac{1}{\kappa_t^2+\kappa_r^2}\right)$, (33) can be rewritten as

$$\mathcal{D}^{\text{wo}}(r_{\text{th}}) = r_{\text{th}}$$
$$\times \left(1 - F_A\left(\sqrt{\frac{1}{\left(1 - (2^{r_{\text{th}}}-1)\left(\kappa_t^2+\kappa_r^2\right)\right)}\frac{2^{r_{\text{th}}}-1}{\tilde{\gamma}}}\right)\right), \qquad (35)$$

where $F_A(\cdot)$ stands for the CDF of A. From (35), it becomes evident that in order to evaluate the achievable throughput, we need first to extract the CDF of A. Towards this direction, from (11), we can rewrite A as

$$A = \sum_{i=1}^{N}\chi_i, \qquad (36)$$

where

$$\chi_i = |h_i|\,|g_i|. \qquad (37)$$

Since $|h_i|$ and $|g_i|$, the PDF of χ_i can be analytically evaluated as

$$f_{\chi_i}(x) = \int_0^{\infty}\frac{1}{y}f_{h_i}(y)f_{g_i}\left(\frac{x}{y}\right)\,\mathrm{d}y, \qquad (38)$$

which, by applying (7) and (8) can be equivalently written as

$$f_{\chi_i}(x) = \sum_{m=1}^{M}\sum_{k=1}^{K}4a_m^{(1)}a_k^{(2)}x^{2b_k^{(2)}-1}\mathcal{I}_{m,k}(x), \qquad (39)$$

where

$$\mathcal{I}_{m,k}(x) = \int_0^{\infty}y^{2b_m^{(1)}-2b_k^{(2)}-1}\exp\left(-c_1y^2 - \frac{c_2x^2}{y^2}\right)\,\mathrm{d}y. \qquad (40)$$

With the aid of [19, Eq. (3.478/4)], (40) can be expressed in closed-form as

$$\mathcal{I}_{m,k}(x) = \left(\frac{c_1}{c_2}\right)^{-\frac{b_m^{(1)}-b_k^{(2)}}{2}} x^{b_m^{(1)}-b_k^{(2)}} \mathrm{K}_{b_m^{(1)}-b_k^{(2)}}\left(2\sqrt{c_1 c_2}x\right).$$
(41)

By applying (41) into (39), we get

$$f_{\chi_i}(x) = \sum_{m=1}^{M}\sum_{k=1}^{K} 4 a_m^{(1)} a_k^{(2)} \left(\frac{c_1}{c_2}\right)^{-\frac{b_m^{(1)}-b_n^{(2)}}{2}} x^{b_m^{(1)}+b_k^{(2)}-1}$$
$$\times \mathrm{K}_{b_m^{(1)}-b_k^{(2)}}\left(2\sqrt{c_1 c_2}x\right),$$
(42)

or

$$f_{\chi_i}(x) = \sum_{m=1}^{M}\sum_{k=1}^{K} a_m^{(1)} a_k^{(2)} \left(\frac{c_1}{c_2}\right)^{-\frac{b_m^{(1)}-b_k^{(2)}}{2}} (c_1 c_2)^{-\frac{b_m^{(1)}+b_k^{(2)}}{2}}$$
$$\times \Gamma\left(b_m^{(1)}\right)\Gamma\left(b_k^{(2)}\right) f_{\mathrm{K}_G}^{(m,k)}(x),$$
(43)

where

$$f_{\mathrm{K}_G}^{(m,k)}(x) = \frac{4\,(c_1 c_2)^{\frac{b_m^{(1)}+b_k^{(2)}}{2}} x^{b_m^{(1)}+b_k^{(2)}-1} \mathrm{K}_{b_m^{(1)}-b_k^{(2)}}\left(2\sqrt{c_1 c_2}x\right)}{\Gamma\left(b_m^{(1)}\right)\Gamma\left(b_k^{(2)}\right)}$$
(44)

Notice that (44) is a special case of the PDF of the generalized-K distribution. Thus, from (43), it becomes apparent that χ_i follows a mixture generalized-K distribution. Likewise, from (36), we observe that A is a sum of N mixture generalized-K distributed RVs; hence, according to [29, Eq. (7)], its CDF can be obtained as

$$F_A(x) = \frac{1}{\Gamma(k_A)\Gamma(m_A)} \mathrm{G}_{1,3}^{2,1}\left(\Xi^2 x^2 \left|\begin{array}{c} 1 \\ k_A, m_A, 0 \end{array}\right.\right),$$
(45)

where (15)–(22) can be extracted by applying [29, Eq. (17)]. Finally, $\mu_{\chi_i}(l)$ can be analytically evaluated as

$$\mu_{\chi_i}(l) = \int_0^\infty x^n f_{\chi_i}(x)\,\mathrm{d}x,$$
(46)

which, by applying (42), can be rewritten as

$$\mu_{\chi_i}(l) = \sum_{m=1}^{M}\sum_{k=1}^{K} 4 a_m^{(1)} a_k^{(2)} \left(\frac{c_1}{c_2}\right)^{-\frac{b_m^{(1)}-b_n^{(2)}}{2}} \mathcal{K}_{m,n},$$
(47)

where

$$\mathcal{K}_{m,n} = \int_0^\infty x^{b_m^{(1)}+b_k^{(2)}+n-1} \mathrm{K}_{b_m^{(1)}-b_k^{(2)}}\left(2\sqrt{c_1 c_2}x\right)\,\mathrm{d}x.$$
(48)

By using [19, Eq. (6.561/16)] in (48), we obtain

$$\mathcal{K}_{m,n} = \frac{1}{4}\,(c_1 c_2)^{-\frac{b_m^{(1)}+b_k^{(2)}+n}{2}}\,\Gamma\left(b_m^{(1)}+\frac{n}{2}\right)\Gamma\left(b_k^{(2)}+\frac{n}{2}\right).$$
(49)

Finally, with the of (49), (47) can be written as (23). Next, by applying (45) into (35) and accounting (34), we obtain (14). This concludes the proof.

APPENDIX B

PROOF OF PROPOSITION 2

In the case the system experiences disorientation and misalignment, by following the same steps as in the Proof of Proposition 1, in the case $\left(2^{r_{\mathrm{th}}}-1\right)\left(\kappa_t^2+\kappa_r^2\right) \leq 1$ the throughput can be expressed as

$$\mathcal{D}^{\mathrm{wo}}(r_{\mathrm{th}}) = 0, \text{ for } r_{\mathrm{th}} \geq \log_2\left(1+\frac{1}{\kappa_t^2+\kappa_r^2}\right).$$
(50)

On the other hand, for $r_{\mathrm{th}} < \log_2\left(1+\frac{1}{\kappa_t^2+\kappa_r^2}\right)$

$$\mathcal{D}^{\mathrm{wo}}(r_{\mathrm{th}}) = r_{\mathrm{th}}$$
$$\times \left(1 - F_{A_{e2e}}\left(\sqrt{\frac{1}{\left(1-\left(2^{r_{\mathrm{th}}}-1\right)\left(\kappa_t^2+\kappa_r^2\right)\right)}\frac{2^{r_{\mathrm{th}}}-1}{\tilde{\gamma}}}\right)\right),$$
(51)

where $F_{A_{e2e}}(\cdot)$ stands for the CDF of A_{e2e}.

To evaluate (51), we first need to find the distribution of A_{e2e}. Since h_g and A are independent RVs, the CDF of A_{e2e} can be written as

$$F_{A_{e2e}}(x) = \int_0^{B_o} F_A\left(\frac{x}{y}\right) f_{h_g}(y)\,\mathrm{d}y.$$
(52)

By employing (3) and (45), (52) can be expressed as

$$F_{A_{e2e}}(x) = \frac{\rho}{B_o^\zeta}\frac{1}{\Gamma(k_A)\Gamma(m_A)}\mathcal{J}(x),$$
(53)

where

$$\mathcal{J}(x) = \int_0^{B_o} y^{\zeta-1}\mathrm{G}_{1,3}^{2,1}\left(\Xi^2\frac{x^2}{y^2}\left|\begin{array}{c} 1 \\ k_A, m_A, 0 \end{array}\right.\right)\,\mathrm{d}y.$$
(54)

With the aid of [30, Eq. (07.34.17.0012.01)], (54) can be equivalently written as

$$\mathcal{J}(x) = \int_0^{B_o} y^{\zeta-1}\mathrm{G}_{3,1}^{1,2}\left(\Xi^{-2}\frac{y^2}{x^2}\left|\begin{array}{c} 1-k_A, 1-m_A, 1 \\ 0 \end{array}\right.\right)\,\mathrm{d}y,$$
(55)

which, by employing [31], yields

$$\mathcal{J}(x) = \frac{B_o^\zeta}{2\zeta}\mathrm{G}_{5,3}^{1,4}\left(\begin{array}{c} 1-k_A, 1-m_A, \frac{1-\zeta}{2}, \frac{2-\zeta}{2}, 1 \\ 0, \frac{1-\zeta}{2}, -\frac{\zeta}{2} \end{array}\left|\frac{B_o^2}{\Xi^2 x^2}\right.\right).$$
(56)

With the aid of (56), (53) can be written as

$$F_{A_{e2e}}(x) = \frac{\zeta}{2\Gamma(k_A)\Gamma(m_A)}$$
$$\times \mathrm{G}_{5,3}^{1,4}\left(\begin{array}{c} 1-k_A, 1-m_A, \frac{1-\zeta}{2}, \frac{2-\zeta}{2}, 1 \\ 0, \frac{1-\zeta}{2}, -\frac{\zeta}{2} \end{array}\left|\frac{B_o^2}{\Xi^2 x^2}\right.\right).$$
(57)

By applying (57) into (51) and combining the resulting formula with (50), we obtain (25). This concludes the proof.

REFERENCES

[1] A.-A. A. Boulogeorgos, A. Alexiou, and M. D. Renzo, "Outage performance analysis of ris-assisted uav wireless systems under disorientation and misalignment," *IEEE Trans. Veh. Technol.*, Jun. 2022.

[2] D. Pliatsios, S. K. Goudos, T. Lagkas, V. Argyriou, A. A. A. Boulogeorgos, and P. Sarigiannidis, "Drone-base-station for next-generation internet-of-things: A comparison of swarm intelligence approaches," *IEEE Open Journal of Antennas and Propagation*, pp. 1–1, Dec. 2021.

[3] G. Geraci and et al., "What will the future of UAV cellular communications be? a flight from 5G to 6G," *ArXiV*, May 2021.

[4] Z. Xiao and et al., "A survey on millimeter-wave beamforming enabled UAV communications and networking," *IEEE Commun. Surveys Tuts.*, pp. 1–1, Nov. 2021.

[5] A.-A. A. Boulogeorgos, J. M. Jornet, and A. Alexiou, "Directional terahertz communication systems for 6g: Fact check: A quantitative look," *IEEE Veh. Technol. Mag.*, pp. 2–10, Dec. 2021.

[6] Y. Zeng and R. Zhang, "Energy-efficient UAV communication with trajectory optimization," *IEEE Trans. Wireless Commun.*, vol. 16, no. 6, pp. 3747–3760, Jun. 2017.

[7] N. Babu and et al., "Cost- and energy-efficient aerial communication networks with interleaved hovering and flying," *IEEE Trans. Veh. Technol.*, vol. 70, no. 9, pp. 9077–9087, Sep. 2021.

[8] A.-A. A. Boulogeorgos, "Interference mitigation techniques in modern wireless communication systems," Ph.D. dissertation, Aristotle University of Thessaloniki, Thessaloniki, Greece, Sep. 2016.

[9] N. Agrawal, A. Bansal, K. Singh, and C.-P. Li, "Performance evaluation of RIS-assisted UAV-enabled vehicular communication system with multiple non-identical interferers," *IEEE Trans. Intell. Transp. Syst.*, pp. 1–12, Nov. 2021.

[10] X. Guo, Y. Chen, and Y. Wang, "Learning-based robust and secure transmission for reconfigurable intelligent surface aided millimeter wave UAV communications," vol. 10, no. 8, pp. 1795–1799, Aug. 2021.

[11] Y. Pan, K. Wang, C. Pan, H. Zhu, and J. Wang, "UAV-assisted and intelligent reflecting surfaces-supported terahertz communications," vol. 10, no. 6, pp. 1256–1260, Jun. 2021.

[12] L. Yang and et al., "On the performance of RIS-assisted dual-hop UAV communication systems," *IEEE Trans. Veh. Technol.*, vol. 69, no. 9, pp. 10 385–10 390, Sep. 2020.

[13] A.-A. A. Boulogeorgos and A. Alexiou, "Coverage analysis of reconfigurable intelligent surface assisted THz wireless systems," *IEEE Open Journal of Vehicular Technology*, vol. 2, pp. 94–110, Jan. 2021.

[14] A.-A. A. Boulogeorgos and et al., "Terahertz technologies to deliver optical network quality of experience in wireless systems beyond 5G," *IEEE Commun. Mag.*, vol. 56, no. 6, pp. 144–151, Jun. 2018.

[15] A.-A. A. Boulogeorgos, S. Goudos, and A. Alexiou, "Users association in ultra dense THz networks," in *IEEE International Workshop on Signal Processing Advances in Wireless Communications (SPAWC)*, Kalamata, Greece, Jun. 2018.

[16] T. Schenk, *RF Imperfections in High-Rate Wireless Systems*. The Netherlands: Springer, 2008.

[17] A.-A. A. Boulogeorgos, V. M. Kapinas, R. Schober, and G. K. Karagiannidis, "I/Q-imbalance self-interference coordination," *IEEE Trans. Wireless Commun.*, vol. 15, no. 6, pp. 4157 – 4170, Jun. 2016.

[18] A.-A. A. Boulogeorgos, P. C. Sofotasios, B. Selim, S. Muhaidat, G. K. Karagiannidis, and M. Valkama, "Effects of RF impairments in communications over cascaded fading channels," *IEEE Trans. Veh. Technol.*, vol. 65, no. 11, pp. 8878 – 8894, Nov. 2016.

[19] I. S. Gradshteyn and I. M. Ryzhik, *Table of Integrals, Series, and Products*, 6th ed. New York: Academic, 2000.

[20] M. Najafi and et al., "Statistical modeling of FSO fronthaul channel for drone-based networks," in *IEEE International Conference on Communications (ICC)*, Kansas City, MO, USA, May 2018.

[21] V. S. Asadchy, M. Albooyeh, S. N. Tcvetkova, A. Dáaz-Rubio, Y. Radi, and S. A. Tretyakov, "Perfect control of reflection and refraction using spatially dispersive metasurfaces," *Phys. Rev. B*, vol. 94, no. 7, p. 075142, Aug. 2016.

[22] A.-A. A. Boulogeorgos and A. Alexiou, "Performance analysis of reconfigurable intelligent surface-assisted wireless systems and comparison with relaying," *IEEE Access*, vol. 8, pp. 94 463–94 483, 2020.

[23] E. Basar, M. D. Renzo, J. D. Rosny, M. Debbah, M.-S. Alouini, and R. Zhang, "Wireless communications through reconfigurable intelligent surfaces," vol. 7, pp. 116 753–116 773, Aug. 2019.

[24] A.-A. A. Boulogeorgos, N. D. Chatzidiamantis, and G. K. Karagiannidis, "Energy detection spectrum sensing under RF imperfections," *IEEE Trans. Commun.*, vol. 64, no. 7, pp. 2754–2766, Jul. 2016.

[25] A.-A. A. Boulogeorgos, N. Chatzidiamantis, G. K. Karagiannidis, and L. Georgiadis, "Energy detection under RF impairments for cognitive radio," in *Proc. IEEE International Conference on Communications - Workshop on Cooperative and Cognitive Networks (ICC - CoCoNet)*, London, UK, Jun. 2015.

[26] A.-A. A. Boulogeorgos, E. N. Papasotiriou, and A. Alexiou, "Analytical performance assessment of THz wireless systems," *IEEE Access*, vol. 7, no. 1, pp. 1–18, Jan. 2019.

[27] A.-A. A. Boulogeorgos and A. Alexiou, "Error analysis of mixed THz-RF wireless systems," *IEEE Commun. Lett.*, vol. 24, no. 2, pp. 277–281, feb 2020.

[28] E. Björnson, M. Matthaiou, and M. Debbah, "A new look at dual-hop relaying: Performance limits with hardware impairments," *IEEE Trans. Commun.*, vol. 61, no. 11, pp. 4512–4525, Nov. 2013.

[29] K. Peppas, "Accurate closed-form approximations to generalised-K sum distributions and applications in the performance analysis of equal-gain combining receivers," *IET Commun.*, vol. 5, no. 7, pp. 982–989, May 2011.

[30] Wolfram Research, Inc., "The Wolfram functions site," http://functions.wolfram.com/07.34.16.0001.01, accessed: 2021-06-08.

[31] ——, "The Wolfram functions site," http://functions.wolfram.com/07.34.21.0084.01, accessed: 2022-01-27.